2016

Experimental Testing and Modeling of 5 kW Oil-Free Open Drive Scroll Expander Using R245fa

Felipe A Accorsi
Ray W. Herrick Laboratories, Purdue University, West Lafayette, Indiana, USA, faccorsi@purdue.edu

Nelson A James
Ray W. Herrick Laboratories, Purdue University, West Lafayette, Indiana, USA, najames@purdue.edu

Eckhard Groll
Ray W. Herrick Laboratories, Purdue University, West Lafayette, Indiana, USA, groll@purdue.edu

William T Horton
Ray W. Herrick Laboratories, Purdue University, West Lafayette, Indiana, USA, wthorton@purdue.edu

James E Braun
Ray W. Herrick Laboratories, Purdue University, West Lafayette, Indiana, USA, jbraun@purdue.edu

Experimental Testing and Modeling of 5 kW Oil-Free Open Drive Scroll Expander Using R245fa

Felipe A. ACCORSI*, Nelson A. JAMES[1], Eckhard A. GROLL[1], James E. BRAUN[1], William T. HORTON[1],

Ray W. Herrick Laboratories, Purdue University
West Lafayette, Indiana, USA

faccorsi@purdue.edu, najames@purdue.edu, jbraun@purdue.edu, groll@purdue.edu, wthorton@ecn.purdue.edu

* Corresponding Author

ABSTRACT

Organic Rankine Cycles (ORC) are thermodynamic power cycles designed to generate work from low temperature heat sources. The low temperature heat input is, typically, between 80 °C to 270 °C. The efficiency of an ORC is highly dependent on the expander characteristics. This article experimentally evaluates the performance of a scroll expander with nominal capacity of 5 kW, built-in volume ratio of 3.5. Tests were conducted in an ORC test-rig using R245fa as the working fluid. The expander was tested over a full performance map consisting of two temperature sources 85°C and 110°C and five expander speeds, from 800 RPM to 3000 RPM.

The scroll expander achieved a maximum isentropic efficiency of 0.58, for a volume ratio of 6.12, at the expander speed of 1600 RPM and temperature source of 110°C. The same temperature source also registered the maximum expander power output, 3.75 kW, at volume ratio of 6.55 and an expander speed of 2500 RPM.

A semi-empirical model was developed to predict the expander output power and isentropic efficiency. The model was in close agreement with the experimental results with a mean deviation of 4.93%, for the expander isentropic efficiency, and 4.23%, for the power output. The semi-empirical model suggests friction and leakage influence efficiency more than any other source.

1. INTRODUCTION

Projections from the Annual Energy Outlook 2015 (AEO 2015) anticipate a 0.3% yearly growth in U.S. energy demand through 2040. However, it predicts that the U.S. total electricity uses grow by an average of 0.8% per year. These projections of rising energy demand are in and of themselves an incentive for research to study ways to increase the efficiency of equipment for power production.

Conventional methods of energy generation are based on the use of limited sources, such as petroleum, natural gas, and coal. Nuclear fission is another traditional source of energy supply, but it has been linked to recent uncertainty and public disapproval regarding the safety of nuclear power plants. In addition, a higher level of awareness among the world population regarding environmental concerns, such as climate change, create considerable pressure for changes in traditional energy conversion, energy efficiency usage and the exploration of renewable sources.

The combination of the projected growth in electricity demand (and energy demand, in general), social concerns regarding climate change and uncertain fluctuations in fossil fuels costs make clear the need for more efficient equipment and an overall improvement in power generation methods. The Organic Rankine Cycle (ORC) is a technology that can use waste heat to produce power and improve the overall efficiency of an existing machine or process.

Rattner and Garimella (2011) assessed the potential of waste heat from U.S. power generation and thermal processes. According to their study, the largest concentration of waste heat is localized in the range of low

temperature sources in the transportation sector, followed by power plants.

Internal combustion engines (ICE) are a large source of waste heat having typical 1st Law efficiencies between 30 and 40 % with the remainder of the input energy dissipated as heat. Song et al. (2014) examined waste heat recovery of a marine diesel engine using ORC technology. Two separated ORC systems with R245fa and benzene as the working fluids were studied to recover waste heat from the jacket cooling water system and engine exhaust gas. They estimated that a total net power output 101.1 kW could be reached with an efficiency increase of 10.2% for the marine diesel engine.

Katsanos et al. (2012) conducted a theoretical study to investigate the potential of an ORC coupled with the exhaust of a six-cylinder heavy-duty two-stage turbocharged truck diesel engine. Using the working fluid R245ca, their study showed that the brake specific consumption improvement ranged from 10.2% at 25% engine load to 8.5% at 100% engine load. Battista et al. (2015) investigated the interaction of an ORC mounted on the exhaust line of a turbocharged IVECO F1C engine. Their study reported some difficulties in recovering heat from the exhaust gases in the evaporator but also showed that the gross benefit of the ORC-based unit power was 4% to 5%. The study mentioned that additional improvement is possible with a model-based control and more efficient expander.

ORCs can utilize other heat sources besides waste heat from internal combustion engines. For example, Borsukiewicz-Gozdur et al. (2014), Oudkerk et al. (2013), Peris et al. (2014) studied ORCs for combined heating and power Generation.; Saitoh et al. (2007) coupled an ORC to a solar source; Hettiarachchia et al. (2007) considered a geothermal source; and Uris et al. (2015) studied biomass sources.

Expanders applied to ORCs, in general, are categorized into two types according to Qiu et al. (2011). One is the dynamic (turbo) machine type, such as an axial turbine expander; the other is a volumetric (displacement) type, such as screw expanders, scroll expanders, and reciprocal piston expanders. According to Zanelli and Favrat (1994), volumetric types are preferable for small- and medium-scale ORCs, whereas turbo machines are typically used for large-scale energy conversion due to higher costs and operation speeds.

More recently, Song et al. (2014) conducted a review of the research status of scroll expanders and cited that scroll expanders are still in the early stages of development. Most of the small capacity ORC studies use scroll compressors adapted to run as an expander. The objective of the study presented in this paper was the evaluation of the performance, power output and isentropic efficiency of a 5kW scroll expander operating with temperature sources (85°C and 110°C) and the application of modeling techniques to the expander that are useful in characterizing isentropic efficiency and power output.

2. EXPERIMENTAL SETUP

The operating principle of a simple ORC includes four major processes. The working fluid evaporates at high pressure using the heat transfer from a heat source. Then, the enthalpy of the working fluid is reduced in an expander producing mechanical work that can be used directly or converted into electricity by an electric generator. The low-pressure fluid leaving the expander is passed to a condenser, where its temperature is reduced and changes phase to liquid. From there, the liquid is pumped back to a higher pressure and fed to the evaporator.

A test-rig with a schematic representation in Figure 1 was used to characterize the performance of a scroll expander in this study. The expander tested was an open-drive expander with a nominal power capacity of 5kW. It was equipped with a magnetic coupling to minimize leakage risks. Its built-in volume ratio was 3.5 and it had a displacement volume of 73.6 cm^3 per revolution. The expander was limited to a maximum inlet pressure of 1380kPa (200PSI), a maximum temperature of 175°C, and a speed in the range of 500 RPM to 3600 RPM. The goal of the experimentation was to determine the device's efficiency and power production under oil-free operation. The sensor types and uncertainties for the test rig are summarized in Table 1.

The heat source was simulated by a water boiler and the tests were conducted with source temperatures of 85°C and 110°C. The test matrix is summarized in Table 2. For each expander speed, the tests began with the lowest pump speed, when the pressures and flow were stable, between 80 RPM to 110 RPM, leading to the lowest pressure ratio for that expander speed. The pump speed was increased incrementally over its range leading to increasing evaporating pressure, decreasing expander inlet superheat and increasing the pressure ratio across the expander. The

tests for each expander speed were considered ended when one of the three scenarios happened:

- the degree of superheat was lower than 3°C;
- the limit of 23 Nm of the torque sensor was reached; or
- the pressure inlet of the expander was close to 1380kPa (200PSI).

This process was repeated for both temperature sources. Table 2 summarizes all speeds in the test matrix. In addition, tests were performed at the speed of 2400 RPM due to this point being close to a filling factor of 1.

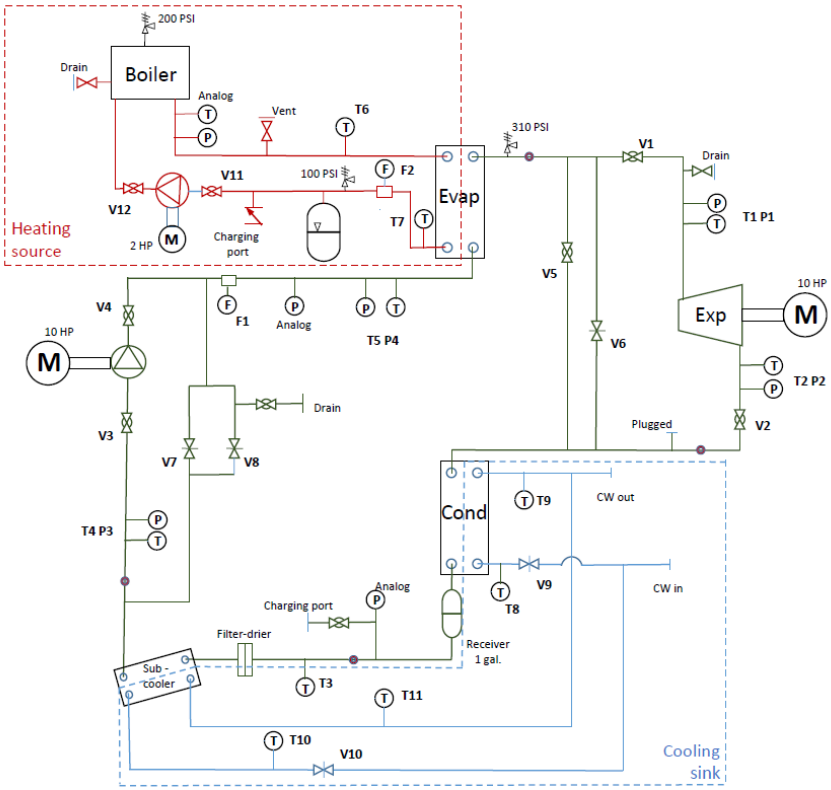

Figure 1: Layout of the ORC test-rig used to test the 5 kW scroll expander.

Table 1: Summary of the sensors and corresponding uncertainties

Measurement	**Description**	**Accuracy**
Temperature	Undergrounded T-Type thermocouple	+/- 0.5°C
Pressure (high-pressure side)	Electronic Pressure Transducer 0-500 psig	+/- 5.65 kPa (+/- 0.82 psi)
Pressure (low- pressure side)	Electronic Pressure Transducer 0-250 psig	+/- 4.105 kPa (+/-0.59 psi)
Mass flow (working fluid)	Coriolis mass flow sensor	+/- 0.1 %
Mass flow (hot water fluid)	Coriolis mass flow sensor	+/- 0.5 %
Torque	Rotating torque sensor	+/- 1.5 %
Shaft Speed	VFD Encoder	+/- 6.84 RPM

The determination of a steady state condition was based on the method developed by Woodland et al. (2012). They proposed a method that compares the average values of the measured variables over windows that are separated by 10 minute intervals. The method is illustrated in Figure 2 and the criteria for steady state are given in Table 3.

Table 2: Test matrix of the expander experimental study.

Source Temperature	Expander Speed (RPM)				
85°C	800	1600	2000	2500	3000
110°C	800	1600	2000	2500	3000

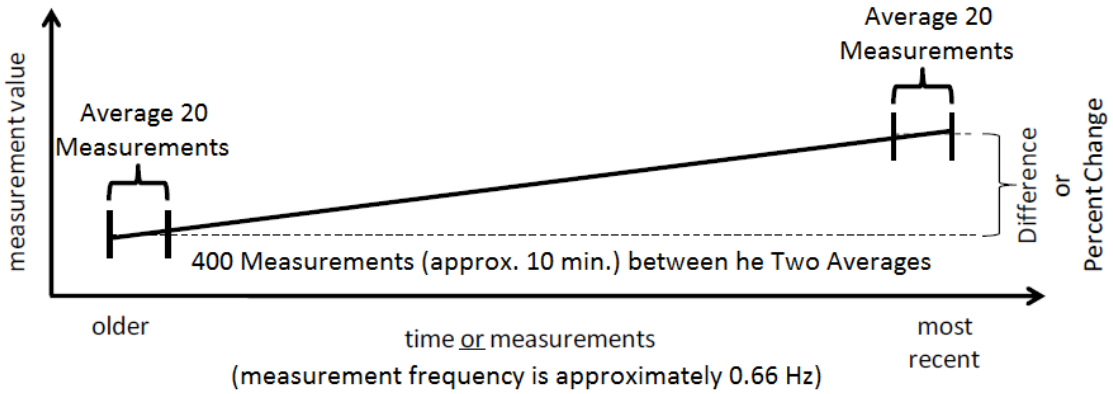

Figure 2: Steady state condition adopted for the experimental evaluation adapted from Woodland et al. (2012).

Table 3: Criteria used in the comparison in each measurement for steady state condition.

Measurement type	**Steady State Criteria**
Temperature	Difference < 0.5 K
Pressure	Change < 2%
Mass Flow	Change < 2%
Rotating Equipment Speed	Change < 2%

The volumetric performance of the scroll expander is quantified using the filling factor (ϕ) defined as the ratio of the actual flow rate to the theoretical flow rate displaced by the expander.

$$\phi = \frac{\dot{m}_{wf} v_{suc}}{N_{shaft} V_{D,exp}} \tag{1}$$

$V_{D,exp}$ is the theoretical displacement volume of the expander The built-in volume ratio (r_v) is a characteristic of the scroll expander dependent on its geometry.

$$r_v = \frac{V_{D,exp}}{V_{D,comp}} \tag{2}$$

The tested expander has a built-in volume ratio of 3.5. The volume ratio imposed on the expander is the ratio of the working fluid specific volume of the expander outlet by the inlet:

$$V_r = \frac{v_{dis}}{v_{suc}} \tag{3}$$

The imposed pressure ratio is calculated in analogous way:

$$P_r = \frac{P_{dis}}{P_{suc}} \tag{4}$$

The overall performance of the expander is evaluated in terms of the expander isentropic efficiency:

$$\eta_{exp} = \frac{\dot{W}_{shaft}}{\dot{W}_s} = \frac{2\pi N_{shaft} \tau_{shaft}}{\dot{m}_{wf}(h_{suc}(T_{suc}, P_{suc}) - h_{dis}(s_{suc}, P_{dis}))} \tag{5}$$

3. EXPERIMENTAL RESULTS

During the experimental test phase, 75 data points were collected. They consisted of 18 points that were run with the temperature source at 85°C, and 57 points from temperature source at 110°C. Figures 3 shows the isentropic efficiency versus volume ratio and filling factor. The peak efficiency of 0.58 occurred at a volume ratio of about 6 and filling factor of about 1.2.

The highest isentropic efficiency found was 0.58 for a temperature source of 110°C, and 0.51 for a temperate source of 85°C. These conditions are summarized in Table 4. The optimal operating efficiencies correspond to filling factors that are slightly greater than one. For the temperature source of 110°C the maximum power production, 3.75 kW, did not coincide with the maximum expander isentropic efficiency. For the temperature source of 85°C, the point of maximum power and efficiency were found to be at the same operating condition. However, it is possible that a larger pressure ratio was necessary to achieve peak efficiency at this operating temperature. The pressure ratio was limited at this condition due to constraints on the operating condition of the test stand.

Table 4: Summary of the conditions for best expander isentropic efficiency and maximum power output.

Temp. Source [ºC]	**Expander Speed** [RPM]	**Degree Superheat** [ºC]	**Pressure ratio** [-]	**Volume Ratio** [-]	**Filling Factor** [-]	**Power** [kW]	**Expander Isen. Eff.** [-]
85.20	2000	1.83	4.80	5.02	1.10	**1.64**	**0.51**
110.41	1600	21.74	5.95	6.12	1.20	2.34	**0.58**
110.19	2500	4.20	5.92	6.55	1.00	**3.75**	0.54

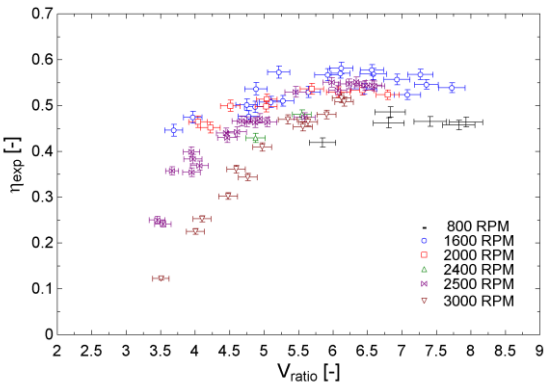

Figure 3: Isentropic Expander Efficiency versus Volume Ratio. Efficiency Peak occurs at volume ratio 6.12. Plot created using all the 75 data points.

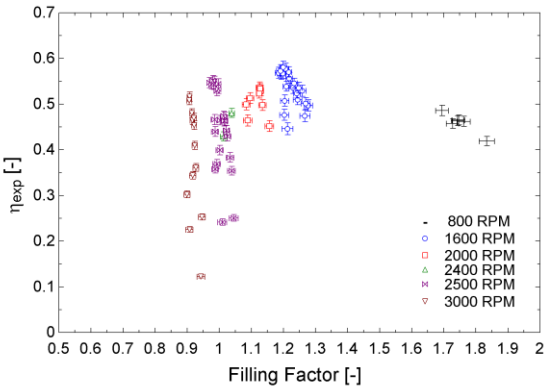

Figure 4: Isentropic Expander Efficiency versus Filling Factor. Efficiency Peak occurs at filling factor of 1.2. Plot created using all the 75 data points.

The expander isentropic efficiency versus pressure ratio is shown for each temperature source in Figure 5 and Figure 6. For the temperature source of 110°C, the expander speed of 1600 RPM consistently shows better efficiency than the other speeds. For the temperature source of 85°C, the expander speed of 2000 RPM yielded higher efficiency than the other speeds. However, close to the expander isentropic efficiency peak of 0.51, the efficiencies at expander speeds of 1600 RPM and 2000 RPM were nearly identical. In both situations, the inlet pressure conditions couldn't be increased due to the degree of superheat at these points. At a speed of 2000 RPM it was 1.83°C and the condensing pressure 155.8 kPa, while for 1600RPM the degree of superheat was 2.4 °C and the condensing pressure 150.2 kPa. However, increasing the pump speed to increase the pressure ratio also elevates the expander inlet pressure and the mass flow rate, which could lead to two phase flow in the expander. An alternative method to test larger pressure ratios for these two speeds would be to lower the condensing pressure. However, the condensing pressure is limited by the sink temperature conditions and since there was no control over the sink water temperature and the flow rate was at a maximum, higher pressure ratios could not be tested.

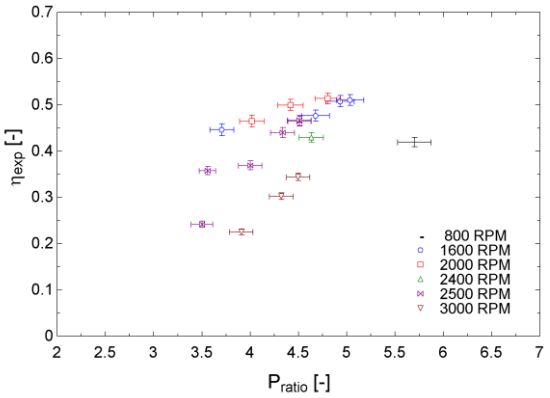

Figure 5: Expander Isentropic Efficiency versus Pressure Ratio for Temperature Source of 85°C.

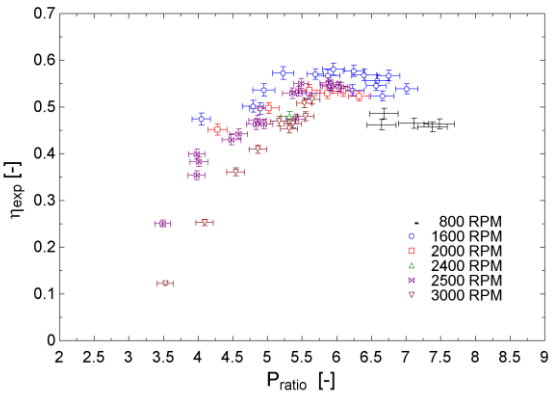

Figure 6: Expander Isentropic Efficiency versus Pressure Ratio for Temperature Source of 110°C.

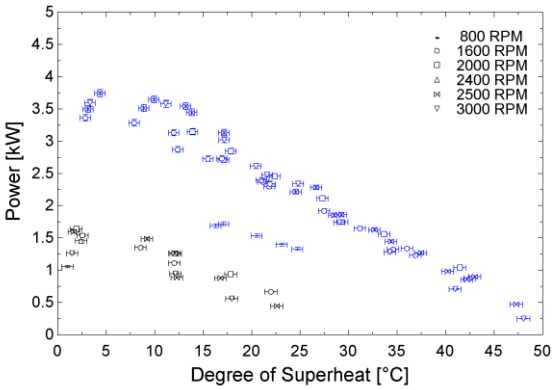

Figure 7: Expander Power Output Versus Degree of Superheat at Expander Inlet. Upper trend represents temperature source of 110°C, while lower trend represents temperature source of 85 °C.

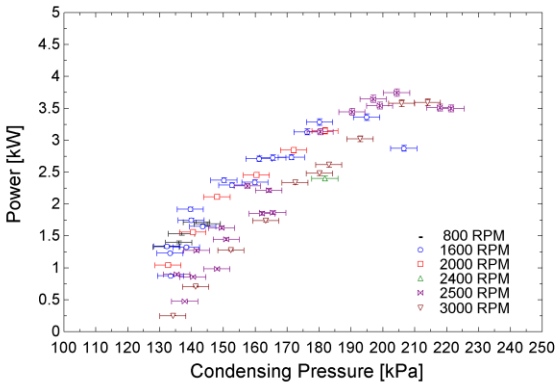

Figure 8: Expander Output Power Versus Condensing Pressure for Temperature Source 110°C.

Figure 7 presents expander power output as a function of inlet superheat. The power output increased with decreasing inlet superheat for all the tested expander speeds but was limited to be greater than zero. Lower inlet superheats are generally associated with higher pump speeds and refrigerant mass flow rates, which lead to higher evaporating pressures. In turn, this leads to higher pressure ratios and density of the working fluid entering this positive displacement expander. Figure 7 shows that the power output is nearly linear with degree of superheat until the superheat approaches zero where power output tends toward a maximum. At this point the pressure ratio across the expander no longer increases with increasing pump speed. This is due to a limitation on the cooling capacity of the test stand. While the evaporation pressure increases due to the increased pump speed and mass flow rate the condensing temperature and hence saturation pressure also increases.

Figure 8 shows power output as a function of condensing pressure for the higher source temperature with a peak output occurring at a condensing pressure of about 200 kPa. This peak power operating point is associated with the maximum pressure ratio over this range of data. There is a maximum pressure ratio for each expander speed for fixed sink conditions (fixed flow rate and condenser inlet temperature). Figure 9 shows that the maximum pressure ratio for the expander speed of 2500RPM occurs at the 200 kPa condensing pressure. The peak occurs because both evaporating and condensing pressures increase with increasing working fluid mass flow rate towards limiting values that depend on the source and sink temperatures but at rates that depend on heat transfer characteristics of the evaporator and condenser.

It should be noted that tests for the expander speed of 800 RPM at a temperature source of 110°C reached the limit of the torque cell. At this point, the superheat was 16.4°C, indicating that higher condensing pressures could have

been tested for this speed if higher rated torque cell were employed.

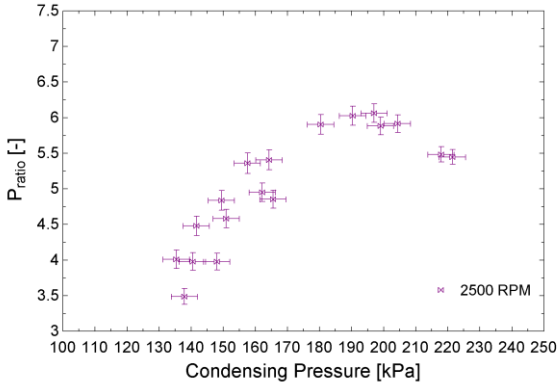

Figure 9: Trend of the Pressure Ratio versus the Condensing Pressure as the Mass Flow Rate Increases.

Table 5: Conditions close to the power limit and minimum degree of superheat.

Expander Expeed [RPM]	**Suc. Pressure** [kPa]	**Dis. Pressure** [kPa]	**P. Ratio** [-]	**Density R245fa** [kg/m^3]	**Temp. Source** [°C]	**Suc. Temp.** [°C]	**Suc. Sat. Temp.** [°C]	**Superheat** [°C]	**Power** [W]
1600	1262.68	180.15	7.01	68.50	109.8	107.66	99.9	7.74	3285.71
1600	1279.89	194.91	6.57	71.97	110.2	103.23	100.5	2.70	3362.33
2500	1170.88	199.01	5.88	61.20	110.2	109.59	96.6	13.03	3545.15
2500	1208.66	204.32	5.92	66.88	110.3	102.17	98.0	4.20	3745.85
3000	1161.90	205.89	5.64	61.43	110.2	107.22	96.2	10.99	3577.71
3000	1183.83	214.00	5.53	65.85	110.4	100.22	97.0	3.17	3593.62

4. Expander Modeling

To complement the experimental evaluation of the scroll expander, an expander model was developed from the data collected. A semi-empirical model is used to evaluate the expander's performance and estimate the expander losses based on the determined parameters.

4.1 Semi-Empirical Model

This section presents the semi-empirical model introduced by Lemort et al (2009) and its application to the scroll expander tested. The model is able to predict power, isentropic efficiency, mass flow and outlet temperature of the expander for different operating conditions. The model considers that one cycle of the scroll expander includes suction, expansion and discharge processes with the following physical phenomena:

- su → su,1: working fluid suction pressure drop;
- su,1 → su,2: isobaric suction heat transfer;
- su,2 → in: isentropic expansion to the built-in volume ratio;
- in → ex,3: adiabatic expansion at constant machine volume;
- ex,2 → ex,1: isobaric discharge heat transfer;
- ex,1 → ex: discharge pressure drop

The model has ten parameters that need to be determined:

$$AU_{amb}, AU_{suc,n}, AU_{ex,n}, \dot{m}_{r,n}, V_{s,exp}, V_{r,in}, \tau_{loss}, A_{thr,leak}, A_{thr,suc}, A_{thr,dis}$$

The parameters of the model are then identified by minimizing a global error function accounting for errors in the prediction of the main output variables of the model (mass flow rate, shaft power and exhaust temperature):

$$error = \sqrt{\sum_{1}^{N_{data}} \left(\frac{\dot{m}_{calc} - \dot{m}_{meas}}{\dot{m}_{calc}}\right)^2} + \sqrt{\sum_{1}^{N_{data}} \left(\frac{\dot{W}_{calc} - \dot{W}_{meas}}{\dot{W}_{calc}}\right)^2} + \sqrt{\sum_{1}^{N_{data}} \left(\frac{T_{dis,calc} - T_{dis,meas}}{T_{dis,calc}}\right)^2} \quad (6)$$

The generic algorithm implemented by James et al. (2015) was used to perform the error minimization using 10 experimental data points. The resulting model parameters are given in Table 6.

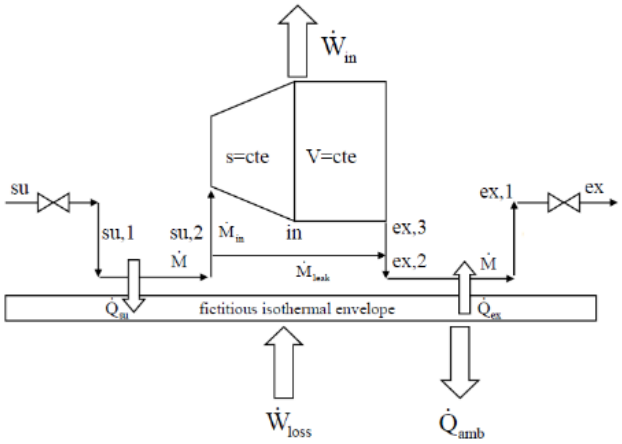

Figure 10: Conceptual scheme of the expander model. Source: Lemort et al (2009)

Table 6: Parameters determined by the minimization of the semi-empirical model.

Semi-Emprical Parameters		
$\dot{m}_{r,n}$	0.1384	[kg/s]
$AU_{suc.n}$	28.3949	[W/K]
$AU_{ex.n}$,	11.7066	[W/K]
AU_{amb}	6.1725	[W/K]
$V_{s,exp}$	8.10E-05	[m^3]
$V_{r,in}$	3.3009	[-]
$A_{thr,suc}$	4.01E-05	[m^2]
$A_{thr,leak}$	7.43E-06	[m^2]
$A_{thr,dis}$	0.000267	[m^2]
τ_{loss}	2.9680	[Nm]

As shown in Figure 11, the semi-empirical model predicts the isentropic efficiency with mean deviation of 4.93 % and a maximum relative error of 17.75% for all the data points. However, the maximum prediction errors for 69 out of the 75 experimental data points are less than 10%. The power output of the expander is predicted with a maximum deviation of 15% and a mean deviation of 4.23%. Figure 12 indicates that the highest relative deviation occurs at low power output of less than 1 kW. For higher output power points, the deviation falls inside 8%.

The mass predictions are in good agreement with the experimental data with a maximum deviation of 8.06% and a mean deviation of 2.2%. However, the model tends to somewhat under predict the mass flow rates at higher values as seen in Figure 13.

Figure 14 shows comparisons of expander outlet temperatures. The model tends to over predict the expander output temperature with a maximum difference of 4.38 K that occurs at the highest temperature. Besides this deviation, all the other 74 data points are predicted with deviation in the interval +3.5 K to -2K. At higher expander speeds the accuracy of the model decreases. High expander outlet temperatures are associated with lower power outlet, and this

deviation for high outlet temperatures agrees with the lower accuracy of the power prediction shown in Figure 12.

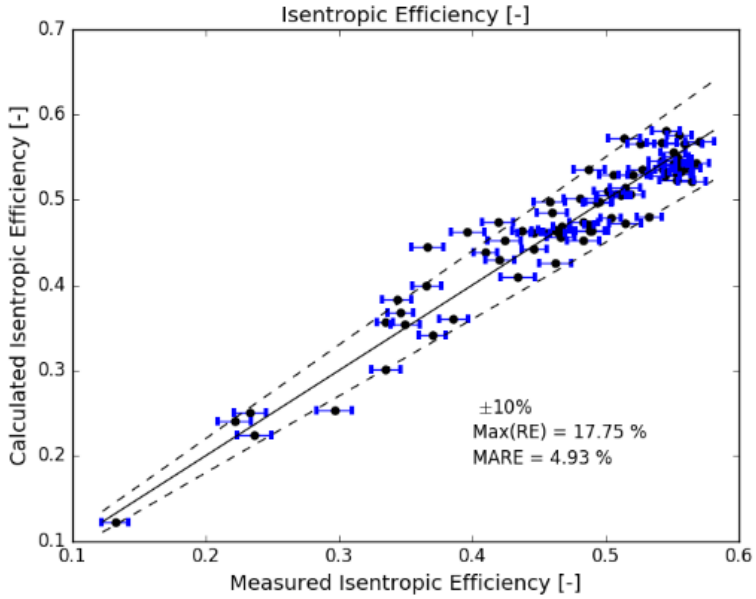

Figure 11: Calculated Isentropic Efficiency versus Measured Isentropic Efficiency of the Semi-Empirical Model with Parameters from Table 6.

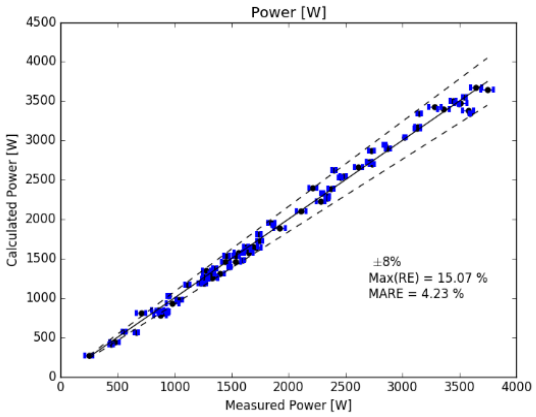

Figure 12: Calculated Output Power versus Measured Output Power of the Semi-Empirical Model with Parameters from Table 6.

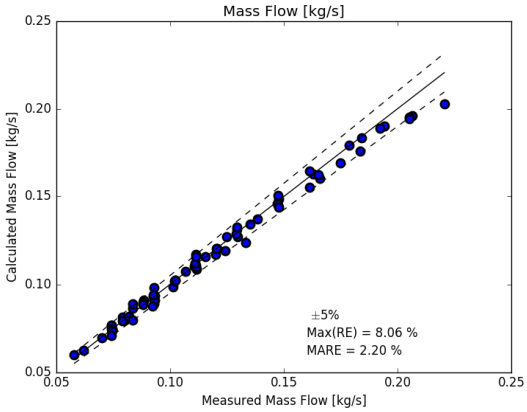

Figure 13: Calculated Mass Flow Rate versus Measured Mass Flow Rate of the Semi-Empirical Model with Parameters from Table 6.

Figure 15 presents model predicted trends of isentropic efficiency for different cases that exclude different types of expander losses. The bottom curve includes all of the losses and then subsequent curves remove sequentially leakage, pressure drop, mechanical, and heat transfer losses. The top curve only includes losses associated with under- or over-compression when the volume ratio is not equal to the built-in volume. For pressure ratios lower than about 5, mechanical losses (friction and bearing losses) have the most significant effect on overall expander performance. These losses cause the location of the expander peak efficiency to shift from its build-in volume ratio to a higher volume ratio that has a corresponding pressure ratio of about 6. The other major source of losses is due to internal leakage, which is leakage between scroll chambers across radial and flank gaps. These losses have the largest relative impacts for pressure ratios above about 5. Losses due to heat transfer are relatively small and could be neglected. Losses due to pressure drop are more important at lower pressure ratios but could be neglected for pressure ratios greater than about 6.

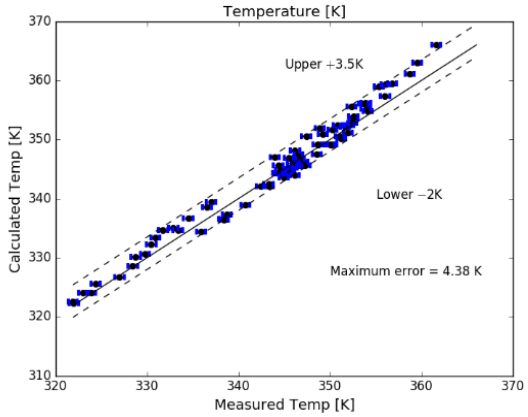

Figure 14: Calculated Outlet Temperature versus Measured Outlet Temperature of the Semi-Empirical Model with Parameters from Table 6.

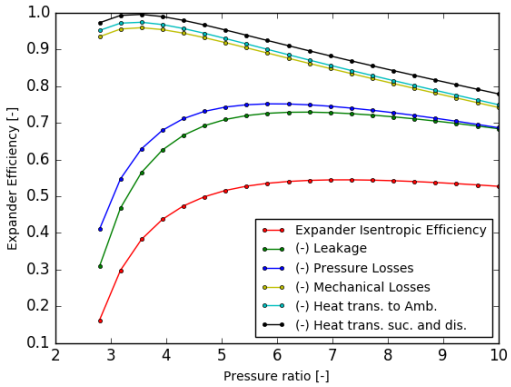

Figure 15: Isentropic Efficiency versus Pressure Ratio. From the Bottom Curve to the Top Curve, The Effects of the Losses Are Shown. Each Curve Accounts for the Loss Effects from its Antecedent Curves**.**

6. CONCLUSIONS

A set of 75 data points were collected to characterize a 5 kW scroll expander's performance for two temperature sources, 85°C and 110°C. Five expander speeds were considered in the test matrix, Table 2. At each expander speed, pump speeds were varied leading to a range of evaporating pressures, condensing pressures, and expander inlet superheat values with limits set on maximum expander inlet pressure, minimum expander inlet superheat, and maximum shaft torque sensor output.

The conditions of maximum measured isentropic efficiency and power output of the expander are summarized in Table 4. The maximum expander isentropic efficiency of 0.58 was measured for an expander speed of 1600 RPM and temperature source of 110°C. The peak efficiency point can also be seen in Figure 3. For the temperature source of 85°C, the maximum expander isentropic efficiency determined during testing and shown in Figure 5 also corresponded to the maximum power output achieved and occurred at the maximum pressure ratio tested for that operating speed. Therefore, it cannot be affirmed that this is the maximum isentropic efficiency for this expander speed without testing larger pressure ratios. Larger pressures ratios were not possible due to constraints imposed by the minimum inlet superheat and the minimum possible condensing pressure associated with the sink temperature.

Although the expander has a rated nominal maximum capacity of 5 kW, the maximum power output obtained during testing was 3.75 kW. To achieve the nominal power capacity, larger pressure ratios would be necessary. This would require either higher source temperatures or lower sink temperatures. The expander is rated for temperatures up to 175°C and could indeed be tested with higher temperature sources. However, the hot water loop in the current test setup would need to be modified, since the current expansion tank is limited it to 115°C.

An optimum pressure ratio for peak efficiency was found for a source temperature of 110°C, but peak efficiency was not achieved for 85°C with the range of conditions tested. The optimum pressure ratio for the lower source temperature could not be achieved because the maximum pressure ratio for the test stand was limited by the control approach.

The semi-empirical modeling approach of Lemort et al (2009) was applied to the scroll expander and accurately characterizes the performance in terms of mass flow rate, power output, and efficiency. The model was used to analyze the major loss mechanisms. For this expander, leakage and mechanical losses have the most significant impact on overall efficiency and therefore should be addressed first in improving performance.

NOMENCLATURE

h	specific Enthalpy	(J/kg)
$\dot{m}$	Mass flow rate	(kg/s)
N	Expander speed	(rev/sec)
P	Pressure	(kPa)
s	Entropy	(J/ kg °C)
T	Temperature	(°C)
V	Volume	(m^3)
v	Specific Volume	(m^3/kg)
$\dot{W}$	Power	(W)
ϕ	Filling Factor	(-)
η	Expander Isentropic Efficiency	(-)
τ-	Torque	(Nm)
AU	Heat Transfer Coefficient	(W/m)
A	Area	(m^2)

Subscript

amb	Ambient
D, exp	Expander displacement expansion volume
$D, comp$	Expander displacement compression volume
Exp	Expander
r	Ratio
r, in	Built-in
s	Isentropic
suc	Suction
thr	Throat
wf	Working fluid

REFERENCES

Battista, D.; Mauriello, M.; Cipollone, R. (2015): Waste heat recovery of an ORC-based power unit in a turbocharged diesel engine propelling a light duty vehicle. *Applied Energy*, *152*, 109–120.

Borsukiewicz-Gozdur, A.; Wisniewski, S.; Mocarski, S.; M. Bankowski (2014): ORC power plant for electricity production from forest and agriculture biomass. *Energy Conversion and Management, 87*, Pages 1180–1185.

Hettiarachchia, H. D. M., Golubovica, M., Woreka, W. M., Ikegamib, Y. (2007). Optimum design criteria for an Organic Rankine cycle using low-temperature geothermal heat sources. *Energy, 9*,1698-1706.

James, N.; Braun, J.; Groll, E.; Travis, W. (2016): Semi-empirical modeling and analysis of oil flooded R410A scroll compressors with liquid injection for use in vapor compression systems.; *International journal of refrigeration, 66*, 50–63.

Katsanos, C.; Hountalas, D.; Pariotis, E. (2012): Thermodynamic analysis of a Rankine cycle applied on a diesel truck engine using steam and organic medium. *Energy Conversion and Management, 60*, 68–76.

Lemort, V.; Quoilin, S.; Cuevas, C.; Lebrun, J. (2009): Testing and modeling a scroll expander integrated into an Organic Rankine Cycle. *Applied Thermal Engineering, 29*, 3094–3102

Oudkerk, J.; Quoilin, S.; Declaye, S.; Guillaume, L.; Winandy, E.; Lemort V. (2013): Evaluation of the Energy Performance of an Organic Rankine Cycle-Based Micro Combined Heat and Power System Involving a Hermetic Scroll Expander. *Journal of Engineering for Gas Turbines and Power, 135*.

Peris, B.; Navarro-Esbrí, J.; Molés, F.; Martí, J. (2015): Mota-Babiloni, A.: Experimental characterization of an Organic Rankine Cycle (ORC) for micro-scale CHP applications. Applied Thermal Engineering, 79, pages 1-8.

Qiu, G.; Liu, H.; Riffat, S. (2011): Expanders for micro-CHP systems with organic Rankine cycle. *Applied Thermal Engineering, 31*, 3301 to 3307.

Rattner, A.; Garimella, S. (2011): Energy harvesting, reuse and upgrade to reduce primary energy usage in the USA. *Energy, 36*, 6172 to 6183.

Saioth, T.; Yamada, N.; Wakashima, S. (2007): Solar Rankine Cycle System Using Scroll Expander. *Journal of Environment and Engineering, 2*, No. 4.

Song, P.; Wei, M.; Shi, L.; Danish, S.; Ma, C. (2015): A review of scroll expanders for organic Rankine cycle systems. *Applied Thermal Engineering*, *75*, 54 to 64.

U.S. Energy Information Administration (20015): Annual Energy Outlook 2015 (AEO2015) – http://www.eia.gov/forecasts/archive/aeo15/

Uris, M., Linares J. I., Arenas, E. (2015): Size optimization of a biomass-fired cogeneration plant CHP/CCHP (Combined heat and power/Combined heat, cooling and power) based on Organic Rankine Cycle for a district network in Spain. *Energy*, *9*,935–945.

Woodland, B.; Braun, J.; Groll, E.; Horton, W. (2012): Experimental Testing of an Organic Rankine Cycle with Scroll-type Expander. *International Refrigeration and Air Conditioning Conference at Purdue, July 16-19*, 2012.

Zanelli, R.; Favrat, D. (1994): Experimental Investigation of a Hermetic Scroll Expander-Generator. *International Compressor Engineering Conference*, Paper 1021.

ACKNOWLEDGEMENT

The financial support from the CAPES Foundation, Ministry of Education of Brazil, is greatly appreciated.